Automatic Defect Inspection for LCDs Using Singular Value Decomposition

by

Chi-Jie Lu and Du-Ming Tsai

Department of Industrial Engineering and Management
Yuan-Ze University, Taiwan, R.O.C.

Correspondence:

Du-Ming Tsai
Department of Industrial Engineering & Management
Yuan-Ze University
135 Yuan-Tung Road
Nei-Li, Tao-Yuan
Taiwan, R.O.C.

Tel: +886-3-4638800
Fax: +886-3-4638907
E-mail: iedmtsai@saturn.yzu.edu.tw

Automatic Defect Inspection for LCDs Using Singular Value Decomposition

ABSTRACT

Thin Film Transistor Liquid Crystal Displays (TFT-LCDs) have become increasingly popular and dominant as display devices. Surface defects on TFT panels not only cause visual failure, but result in electrical failure and loss of LCD operational functionally. In this paper, we propose a global approach for automatic visual inspection of micro defects on TFT panel surfaces. Since the geometrical structure of a TFT panel surface involves repetitive horizontal and vertical elements, it can be classified as a structural texture in the image. The proposed method does not rely on local features of textures. It is based on a global image reconstruction scheme using the singular value decomposition (SVD). Taking the image as a matrix of pixels, the singular values on the decomposed diagonal matrix represent different degrees of detail in the textured image. By selecting the proper singular values that represent the background texture of the surface and reconstructing the matrix without the selected singular values, we can eliminate periodical, repetitive patterns of the textured image, and preserve the anomalies in the restored image. In the experiments, we have evaluated a variety of micro defects including pinholes, scratches, particles and fingerprints on TFT panel surfaces, and the result reveals that the proposed method is effective for LCD defect inspections.

Keywords: LCDs, defect inspection, singular value decomposition, machine vision

1. INTRODUCTION

Thin Film Transistor Liquid Crystal Displays (TFT-LCDs) have become increasingly important in recent years due to their full-color display capabilities, low power consumption and small size. In order to monitor the process stability and guarantee the display quality of LCD flat panels, the inspection of defects on the TFT panels becomes a critical task in manufacturing. Human visual inspection and electrical functional tests are the most commonly used methods for LCD defect detection. However, manual inspection is a time consuming and tiresome task. The manual activity of inspection could be subjective and highly dependent on the experience of human inspectors. The electrical functional test is inherently limited to offline operations, and generally can only be accomplished after the fabrication of a TFT panel is complete. In this paper, we propose an automatic visual system for LCD defect inspections.

Surface defects of the TFT panel not only cause visual failure but also cause electrical failure to operate an LCD panel. Appearance defects on TFT panels can be roughly classified into two categories, macro and micro defects [12]. Macro defects include “MURA”, “SIMI” and “ZURE”. “MURA” means unevenness of a TFT panels. “SIMI” mean stains on a TFT panel. “ZURE” means misalignment of a TFT panel. Micro defects include pinholes, fingerprints, particles and scratches. The macro defects appear as high contrast regions with irregular sizes and shapes. They are generally large in size and, therefore, can be easily detected by human inspectors. However, sizes of micro defects are generally very small and can not be easily found by human inspectors or detected with electrical methods. The proposed method in this paper especially focuses on the inspection of micro defects by utilizing the structural features of TFT panels.

Regarding automatic inspection systems for LCDs, several electrical or optical based inspection techniques have been developed for LCD manufacturing [3,7,18,25]. Henly and Addiego [5] used a 2-D electro-optic modulator to generate voltage images, which measured the surface potential of the LCD panel in a non-contact manner. Kido et al. [26] presented an optical charge sensing technique for partially completed active-matrix LCD panels. Surface reflection was used to sense optical changes and to generate a map that shows the type and location of line and point defects. Most existing methods of automatic inspection systems for LCDs are based on conventional electrical methods to detect the surface potential. Those electrical methods work well for functional verification of a TFT panel. As aforementioned, they can only be accomplished after the fabrication is completed. In-process inspection may not be possible with the functional test approach.

A few vision-based techniques that use pattern-matching algorithms were developed for LCDs inspection. Nakashima [12] presented an inspection system based on image subtraction and optical Fourier filtering for detecting defects on an LCD color filter panel. The image subtraction method was utilized to detect white and black defects such as black matrix holes and particles, and the Fourier filtering was applied for grain defects. Sokolov and Treskunov [24] developed an automatic vision system for final output check of LCDs. For defect detection they compared brightness distributions between a reference LCD image and a test image. The existing vision-based techniques generally need a pre-stored reference image for comparison. This requires a large volume of data for reference and precise environmental controls such as alignment and lighting for test images. Moreover, the techniques for LCD inspection mainly focus on final appearance checks for defects such as nap or dark/bright spots after the fabrication is completed.

A TFT panel generally involves repetitive horizontal gate lines and vertical data lines. Since the geometrical structure of a TFT panel surface involves these horizontal and vertical elements, it can be classified as a structural texture in the image. The textural feature of a TFT panel surface results in a homogeneous image that consists of an arrangement primarily of horizontal and vertical lines appearing periodically on the surface. Since singular value decomposition (SVD) of a matrix involves horizontal and vertical basis functions, it is well suited for representing the structural features of TFT panels. In this study, we use the SVD-based image reconstruction technique to detect the micro defects on TFT panel surfaces.

The SVD method was first proposed in the 1970s and has been applied in a wide range of computer vision applications such as image hiding [14,21], image restoration [10,11,16], and image compression and reconstruction [1,2,9,15,19,20,22,27,28]. For image compression and reconstruction applications, the SVD-based methods were mainly applied to extract the significant feature components of the image. The global, main information of the image is mostly concentrated within a certain number of singular values with related singular vectors. Only the relevant parts of the singular values and related singular vectors need to be retained as the compressed data for reconstructing the original images. The local, detailed information can be truncated to eliminate the redundancy of image compression.

A few studies have been done with the use of the SVD for texture analysis in computer vision. Luo and Chen [8] utilized the SVD for texture discrimination. They used the proportion of dominant singular values of an image matrix as textural features to discriminate textures. Hatipoglu and Mitra [23] combined Teager filters and the SVD for texture feature extraction. Teager filters were first used to find the local energy values and provide efficient feature vectors. The filter outputs were then

combined with the eigenvalues obtained from the SVD of local image partitions to form feature vectors. Kvaal et al. [13] used the SVD for feature extraction from the image of bread. They applied the SVD to extract the singular values of each inspected image and to form an SV-spectra matrix. Then, the SV-spectra matrix was used to classify the sensory porosity of wheat baguettes.

The aforementioned SVD-based methods for texture analysis generally use singular values or singular vectors derived from a textured image to characterize the textural features, and then use complicated classifiers to segment or classify textures. However, different textures may need different textural features to describe the textural patterns. The feature extraction process for a best set of textural features is generally carried out by trial and error, and may highly rely on human expertise.

In this paper, we propose a global approach that uses an SVD-based image reconstruction technique for inspecting micro defects including pinholes, scratches, particles and fingerprints on the surface of TFT panels. The proposed method does not rely on textural features to detect local anomalies, and does not require a reference image for comparison. It alleviates all limitations of the feature extraction schemes and template matching methods just mentioned.

The SVD can be used to decompose an image and obtain a diagonal matrix. The ordered entries of the diagonal matrix are singular values. The main information, or the approximation, of an image can be represented by a few singular values with large magnitude. The remaining singular values with small magnitude provide detailed information of the image. Since the TFT panels contain periodical horizontal and vertical structures, the larger singular values retain the information of the repetitive structural pattern of a TFT panel, and the smaller singular values are associated with anomalies in the TFT panel. In the application of LCD defect inspection, we can set

the larger singular values to zero and preserve the smaller singular values to reconstruct the image. The background texture will be removed and anomalies can be distinctly enhanced in the restored image accordingly.

The SVD is ideally suited for describing the orthogonal pattern in a gray-level image. By considering an input image as a matrix, the SVD process decomposes the image into the eigenvalue-eigenvector factorization. We first select the proper number of larger singular values to represent the repetitive, orthogonal structure features of a TFT panel. Then, we set the selected singular values to zero and reconstruct the image. For a faultless TFT panel, the reconstruction process will result in a uniform image. For a defective TFT panel, the anomalies will be preserved and the periodical patterns of the horizontal and vertical lines will be eliminated on the restored image. Finally, the statistical process control principle is used to set the threshold for distinguishing between defective regions and uniform regions in the restored image.

This paper is organized as follows: Section 2 first discusses the structural characteristics of TFT panel surfaces, and describes the properties of the SVD. The selection of the proper number of larger singular values, and the image reconstruction scheme for LCD defects inspection, are then thoroughly described. Section 3 presents the experimental results from a variety of LCD micro defects. Sensitivity of changes in image rotation and the sensitivity of the selective number of singular values are also evaluated in this section. The paper is concluded in section 4.

2. THE DEFECT DETECTION SCHEME

2.1 The Structural Pattern of a TFT panel

A TFT panel generally contains horizontal gate lines on one plane and vertical data lines on the other plane. At each pixel, the gate of the TFT is connected to the gate line and the source is connected to the data line. Figure 1 shows the schema of a single pixel of a typical TFT panel [26]. Since the TFT panel is comprised of horizontal gate lines and vertical data lines, it forms a structural texture that contains horizontal and vertical line patterns. The structurally textured image of a TFT panel is shown in Figure 2.

2.2 Singular Value Decomposition

Consider an input image of size $M \times N$ as a matrix X of dimensions $M \times N$, where $M \geq N$. It is possible to represent this image in the r-dimensional subspace, where r is the rank of X, and $r \leq N$. The SVD [6] is a factorization of a matrix X into orthogonal matrices,

$$X = USV^T \tag{1}$$

where U is an $M \times r$ matrix and consists of the orthonomalized eigenvectors of XX^T, V is an $N \times r$ matrix and consists of the orthonomalized eigenvectors of $X^T X$. S is an $r \times r$ diagonal matrix consisting of the "singular values" of X, which are the nonnegative square roots of the eigenvalues of $X^T X$. These singular values, denoted by σ, are sorted in non-increasing order, i.e., $\sigma_1 \geq \sigma_2 \geq \cdots \geq \sigma_r \geq 0$.

The SVD is based on orthonormal bases for decomposing the matrix X [17]. The singular values (σ) represent the energy of matrix X projected on each

subspace. The singular values and their distribution, which carry useful information about the contents of X, vary drastically from image to image. For an image with orthogonal texture content such as horizontal and/or vertical structures, only a very few larger singular values will dominate, and yet all others have magnitudes close to zero. Figure 3 shows two artificial images and a TFT panel image and their corresponding first ten singular values. Both artificial images in Figures 3(a) and (b) contain well-structured lines with different line spacing. Figure 3(c) is a real TFT panel image. All three images contain horizontal and vertical lines patterns. From Figure 3, we can observe that the first (the largest) singular value dominates all other singular values, which decrease to zero rapidly.

In most of the cases, the larger singular values (with lager magnitude) represent the global approximation of the original image. All other smaller singular values provide the local, detailed information of the image. Therefore, we can select the proper number of larger singular values to represent the global, repetitive textural feature of the image and remove such background texture by reconstructing the image without the use of larger singular values.

2.3 SVD-Based Image Reconstruction

In this study, we use machine vision to tackle the problem of detecting micro defects including pinholes, scratches, particles and fingerprints which appear as local anomalies in TFT panels. The SVD has desirable properties of orthogonal bases to deal with the orthogonal textural feature of TFT panel surfaces. Therefore, the SVD-based image reconstruction technique is used to remove the orthogonal line patterns in TFT panel surfaces. With this approach, we do not have to define various features for different types of defects. For defect detection purposes, the SVD-based

image reconstruction scheme simply eliminates all repetitive horizontal and vertical patterns of TFT panels. What is retained in the resulting image can then be easily identified as defects on the TFT panels.

The image reconstructed from the selective singular values is given by

$$\hat{X} = \sum_{j=k+1}^{r} \sigma_j U_j V_j^T \tag{2}$$

where $\hat{X}$ is the reconstructed image, U_j and V_j are jth column vectors of U and V, respectively; k is some selected number of singular values; σ_j is jth singular value of S, and r is the rank of the matrix X.

For the image compression and reconstruction application, we can preserve only the k largest singular values to closely approximate the original image. Figure 4 shows an artificial orthogonal-lines image and its reconstructed images. Figure 4(a) shows the original image containing horizontal and vertical lines. Figures 4(b1) and (b2) show the images reconstructed from individual σ_1 and σ_2, respectively. It can be observed that the reconstructed image from sole σ_1 or σ_2 alone can not sufficiently represent the texture feature of the original image. It can be seen from Figure 4(b3) that the reconstructed image from the first two largest singular values (both σ_1 and σ_2) can well represent the original image (Fig. 4(a)). Note that the image size in Figure 4 is 256×256, and there are a total of 256 singular values. Only the first two largest singular values, σ_1 and σ_2, dominate the global, repetitive texture of the line pattern.

On the other hand, in the defect inspection application, we can set the proper number of larger singular values (from σ_1 to σ_k) to zero and preserve the smaller

singular values to reconstruct an image. The background texture will be removed and the defects will be preserved if they exist. Figures 4(c1)-(c3) illustrate the reconstructed images by excluding the singular values with larger magnitude. Figure 4(c1) shows the reconstructed image by excluding the largest singular value σ_1, and Figure 4(c2) shows the resulting image by excluding the second largest singular value σ_2. It can be seen that solely setting σ_1 or σ_2 to zero cannot sufficiently eliminate the background texture in the reconstructed image. Figure 4(c3) demonstrates the reconstructed image by excluding both σ_1 and σ_2 simultaneously. We can observe that the resulting image is approximately a uniform black image for the original faultless image.

2.4 Selecting the Proper Number of Singular Values

When using the SVD image reconstruction scheme for defect detection, we first use Eq. (1) to decompose the image and obtain a set of singular values. Then, we need to select the proper number (i.e., the parameter k in Eq. (2)) of singular values, which can sufficiently represent the repetitive structural pattern, and use Eq. (2) to reconstruct the image. In this study, the proper number k is determined by the difference between two adjacent singular values σ_i and σ_{i+1}. The difference can be considered as the degree of significance of σ_{i+1} with respect to σ_i. Since various images have a different spread of ranges of magnitudes of singular values (see Fig. 3(d)), it is difficult to determine a suitable threshold directly from the difference between σ_i and σ_{i+1} for the selection of the proper number k. In order to find the proper value of the threshold and to accommodate various images, singular values of each image under inspection must be normalized. The normalization proceeds as

follows:

$$\sigma_i^{'} = \frac{\sigma_i - \mu_\sigma}{s_\sigma}, \quad i = 1,2,...,r \tag{3}$$

where $\sigma_i^{'}$ is the *ith* normalized singular value, σ_i is the *ith* singular value, μ_σ is the mean and s_σ is the standard deviation of all singular values for a given image.

Let $\Delta\sigma_i = \sigma_i^{'} - \sigma_{i+1}^{'}$, which represents the normalized marginal gain of energy at singular value number i. If $\Delta\sigma_i$ is larger than some threshold ($T_{\Delta\sigma}$), the additional singular value σ_{i+1} is considered to be significant. It must also contribute significant energy of the repetitive horizontal and vertical background texture. In that case, it should be excluded in the reconstruction process.

Figure 5(a) represents an artificial structural image that contains two scratch defects. Figure 5(b) shows the plot of the marginal gain ($\Delta\sigma$) of the normalized singular values of the image in Figure 5(a). It can be observed from Figure 5(b) that the marginal gains decrease rapidly to zero after the stable point and become steady afterwards. Thus, the value at the stable point can be used as a threshold ($T_{\Delta\sigma}$) to determine the proper number of singular values that contribute in a major way to the background texture. For Figure 5, the proper number is 4 (k =4), i.e., σ_1, σ_2, σ_3 and σ_4 should be excluded for image reconstruction.

Once the proper number of singular values is selected, we can eliminate the background texture and preserve the defects by excluding the first k largest singular values in Eq. (2). The reconstructed image in Figure 5(c) shows that the resultant region associated with the repetitive line pattern becomes approximately uniform and local anomalies of scratches are well preserved in the reconstructed image.

Since the intensity variation in the background region is very small in the

reconstructed image, we can use the statistical process control principle to set up the control limits for distinguishing defects from the uniform region. The upper and lower control limits for intensity variation in the reconstructed image are given by

$$\mu_{\hat{X}} \pm t \cdot s_{\hat{X}} \tag{4}$$

where, $\mu_{\hat{X}}$ and $s_{\hat{X}}$ are the mean and standard deviation of gray levels in the restored image $\hat{X}$; and t is a control constant. According to the Chebyshev's theorem [4], the probability that any random variable x will fall within t standard deviations of the mean is at least $1-\frac{1}{t^2}$. That is,

$$p(\mu_{\hat{X}} - t \cdot s_{\hat{X}} < x < \mu_{\hat{X}} + t \cdot s_{\hat{X}}) \geq 1 - \frac{1}{t^2}$$

In TFT panel manufacturing, the size of a micro defect is generally small with respect to the whole sensed image. In this study, we set the control constant to $t = 4$, which corresponds to 93.75% for pixels falling within the control limits.

If a pixel with its gray level falls within the control limits, the pixel is classified as a homogeneous element of the background region. Otherwise, it is classified as a defective element. Figure 5 (d) depicts the defect detection result of Figure 5 (c) as a binary image. It shows that the two scratches in the original image are correctly presented in the resulting binary image.

3. Experiments and Discussion

3.1 Experimental Results

In this section, we present experimental results from a variety of micro defects including pinholes, scratches, particles and fingerprints on TFT panel surfaces to evaluate the performance of the proposed defect detection scheme. The test images are 256×256 pixels wide with 8-bit gray levels. Figures 6(a)-(c) show respectively three defective images containing pinhole, scratch and particle blemishes on TFT panel surfaces under a fine image resolution (60 pixels/mm). Figure 7 shows a fingerprint defect under a coarser image resolution (20 pixels/mm). The pinhole, scratch and particle defects can only be detected in images of fine resolution, whereas the fingerprint defect can only be observed in images of coarse resolution.

Figures 8(a)-(d) depict the plots of marginal gain ($\Delta\sigma$) of the four test images shown in Figures 6(a)-(c) and Figure 7, respectively. It can be observed from Figure 8 that if the marginal gains are less than 0.05, they rapidly decrease approximately to zero and become steady afterwards. The singular values with $\Delta\sigma$>0.05 sufficiently represent the orthogonal structure pattern of a TFT panel surface.

Table 1 summarizes the detailed information about the normalized singular values and their marginal gains of the four defect images in Figures 6(a)-(c) and Figure 7. It can be seen from the table that the marginal gains greater than 0.05 are fluctuant and drop rapidly, whereas those smaller than 0.05 will steadily decrease and approximate to zero afterwards. Therefore, 0.05 is the threshold ($T_{\Delta\sigma}$=0.05) of the marginal gain ($\Delta\sigma$) used in this study to determine the proper number of singular values for defect detection in TFT panel surfaces. The numbers of singular values selected for pinholes (Fig. 6(a)), scratches (Fig. 6(b)), particles (Fig. 6(c)) and

fingerprints (Fig. 7) images are 5, 8, 4 and 6, respectively, based on the resulting statistics in Table 1.

Figures 9(a1), (b1), (c1) and (d1) show the defect images of the TFT panel surfaces in Figure 6(a)-(c) and Figure 7, respectively. Figure 9(a2) shows the reconstruction result by setting the first five largest singular values (i.e., $\sigma_1, \sigma_2, \cdots, \sigma_5$) to zero for the pinhole defective image with (Fig. 9(a1)). It can be found that the repetitive structural texture becomes an approximately uniform gray-level region and the abnormal pinhole is well enhanced in the restored image. Figures 9(b2) and (c2) show the reconstruction results of the defective images with scratch (Fig. 9(b1)) and particle (Fig. 9(c1)) by setting the first eight (i.e., $\sigma_1, \sigma_2, \cdots, \sigma_8$) and the first four (i.e., $\sigma_1, \sigma_2, \cdots, \sigma_4$) singular values to zero, respectively. They also reveal that the scratch and particle defects are well preserved in the restored images. Figure 9(d2) illustrates the restored image of Figure 9(d1) by setting the first six singular values (i.e. $\sigma_1, \sigma_2, \cdots, \sigma_6$) to zero. The fingerprint is also distinctly enhanced in the restored image. Figures 9(a3)-(d3) show the defect detection results of Figures 9(a1)-(d1) as binary images, of which the control constant $t = 4$ is used for all test images. It can be seen that the orthogonal texture patterns on the TFT panel surfaces are eliminated and defects are distinctly preserved.

In order to test the robustness of the proposed method, the detection result of a faultless TFT panel surface is also evaluated. Figure 10(a) shows a faultless version of the image in Figure 6, and Figure 10(b) depicts its corresponding marginal gain ($\Delta\sigma$). Table 2 summarizes the faultless image's detailed statistics for the normalized singular values and their marginal gains. Based on the threshold ($T_{\Delta\sigma}$=0.05) selected before, it can be observed from Figure 10(b) and Table 2 that the proper number of singular values are six ($k = 6$). Figure 10(c) shows the restored image by setting the first six

largest singular values (i.e., $\sigma_1, \sigma_2, \cdots, \sigma_6$) to zero. The restored image of the faultless surface is approximately a uniform gray-level image. As seen in Figure 10(d), the resulting binary image of the faultless surface is uniformly white. No defect is claimed in the resulting image for the faultless sample.

3.2 Effect of Varied Number of Singular Values

The number of singular values, k, determines how many singular values will be used to represent the background texture. Too many selected singular values will remove both background texture and local anomalies in the restored image, and may overlook subtle defects. However, too few selected singular values cannot completely remove the background texture in the restored image and may result in false alarms. The test image in Figure 7 is used as the sample to evaluate the effect of varied numbers of singular values on detection results.

As mentioned, we use the threshold $T_{\Delta\sigma}$=0.05 to determine the proper number of singular values. In this experiment, we have examined eight different numbers in the neighborhood of the selected number of singular values k, i.e., $k \pm i$ for i = 1, 2, 3, 4. Figure 11(a) presents the restored image of Fig. 7 by excluding the first six largest singular values (i.e., $k = 6$). Figures 11(b)-(e) show the restored images of Figure 7 with selected numbers 5, 4, 3, and 2, respectively. When the selected number of singular values is not sufficient, the background texture residuals may be retained in the restored image. They have no effect on the local defects. It can be seen from Figures 11(b) and (c) that the background texture can also be sufficiently removed in the restored image for the numbers of singular values $k-1$ and $k-2$ However, Figures 11(d) and (e) show that the residuals of repetitive horizontal and vertical lines patterns along with the defects are retained in the restored images.

Figures 11(f)-(i) show the restored images of Figure 7 with selected numbers 7, 8, 9, and 10, respectively. When the selected number of singular values is more than required, the local defects will be blurred and better uniformity of the background texture will be generated in the restored image. It can be seen from Figures 11(f) and (g) that the restored images of the TFT panel surface can still well enhance the defects. However, Figures 11(h) and (i) show that the defects become blurred with the increasing numbers of singular values $k+3$ and $k+4$.

Based on the result from Figure 11, we can find that $k \pm 2$ will not affect the result of an LCD defect inspection. The restored images of defective surfaces can still effectively remove the background texture and well preserve defects. The selection procedure for the number of singular values along with the tolerance of SVD image reconstruction make the proposed method practical for defect detection in TFT panels.

3.3 Effect of Image Rotation

The SVD is based on the orthogonal bases used to decompose a matrix. The orthogonal bases are sensitive to the rotation of an image. The test image in Figure 6(b) is used as the sample to evaluate the effect of rotation on detection results. The test image is rotated by 1°, 2°, 3°, 4° and 5°.

Figures 12(a)-(f) present the restored images in varied angles of the test image in Figure 6(b). Figure 12(a) shows the restored image of the original image in Figure 6(b) without rotational change. It can be observed from Figures 12(b) and (c) that the restored images of the TFT panel surface can still well enhance the defects with a few random noisy points when the rotation angles are not larger than 2°. However, when the rotation angles are larger than 2°, the residuals of repetitive vertical line patterns

along with the defects are retained in the restored images, as seen in Figures 12(d)-(f). The larger the rotation angles, the more residuals of structural lines are preserved in the resulting images.

Based on the results from Figure 12, we find that 2 degrees is the acceptable rotation for LCD defect inspection. When rotation angles of a sensed image are smaller than 2 degrees, the restored image of a defective surface can still effectively remove the background texture. Conversely, if the rotation angles are greater than 2 degrees, the restored images will contain many structural background noisy points and may result in false rejection of a faultless image. In LCD manufacturing, the TFT panels are generally well aligned. The 2°-rotation restriction of the SVD-based machine vision scheme will not affect the detection performance in practice.

4. CONCLUSIONS

Surface defects on TFT panels not only cause visual failure, but result in electrical failure and loss of LCD operational functionally. In this paper, we have presented a global approach for automatic visual inspection of micro defects on TFT panel surfaces. The proposed method does not rely on the conventional electrical and feature extraction methods to detect defects. It is based on an image reconstruction scheme using singular value decomposition. The SVD approach decomposes an image into the eigenvalue-eigenvector factorization. The SVD orthogonal bases can well represent the horizontal and vertical structures of a TFT panel. By selecting the proper number of singular values on the diagonal matrix and reconstructing the image without the use of the selected singular values, we can eliminate global repetitive patterns of the structurally textured image, and preserve local anomalies in the reconstructed image.

In the experiments, we have evaluated a variety of micro defects including pinholes, scratches, particles and fingerprints on TFT panel surfaces. The experimental results have concluded that 0.05 is a well-suited threshold of marginal gains ($\Delta\sigma$) to determine the proper number of larger singular values that contribute to the repetitive background texture. The experiments also show that the selected number k of larger singular values can tolerate minor variation without affecting the reconstruction result. The experiment on the effect of rotation has shown that the tolerable rotation angles of the proposed method are 2 degrees. The proposed SVD-based machine vision scheme has shown promising results for micro defects inspection of TFT panels.

REFERENCES

1. B. Cagnoli and T. J. Ulrych, Singular value decomposition and wavy reflections in ground-penetrating radar image of base surge deposits, Journal of Applied Geophysics, 48, pp. 175-182, 2001.
2. B. P. Popesuc, J. C. Pesquet and A. P. Petropulu, Joint singular value decomposition-a new tool for separable representation of image, IEEE International Conference on Image Processing, 2, pp. 569-572, 2001.
3. C. S. Lin, W. Z. Wu, Y. L. Lay and M. W. Chang, A digital image-based measurement system for a LCD backlight module, Optics and Laser Technology, 33, pp. 499-505, 2001.
4. D. R. Anderson, D. J. Sweeney and T. A. Williams, Statistics for Business and Economics, South-Western, Cincinnati, Ohio, 2002.
5. F. J. Henly and G. Addiego, In-line functional inspection and repair methodology during LCD panel fabrication, 1991 SID Symposium Digest Paper, 32, pp. 686-688, 1991.
6. G. Strang, Introduction to Linear Algebra, Wellesley-Cambridge Press, Wellesley, MA, 1998.
7. H. Jeff, Electro-optics technology tests flat-panel displays, Laser Focus World, 36, pp. 271-276, 2000.
8. J. H. Luo and C. C. Chen, Singular value decomposition for texture analysis, Proceedings of SPIE-The International Society of Optical Engineering, Vol. 2298, Applications of Digital Image Processing XVII, San Diego, CA, USA, pp. 407-418, 1994.
9. J. J. Wei, C. J. Chang, N. K Chou and G. J. Jan, ECG data compression using truncated singular value decomposition, IEEE Transactions on Information Technology in Biomedicine, 5, pp. 290-299, 2001.
10. K. Konstantinides and G. S. Yovanof, Application of SVD based spatial filtering to video sequences, IEEE International Conference on Acoustics, Speech and Signal Processing, Detroit, MI, 4, pp. 2193-2196, 1995.
11. K. Konstantinides, B. Natarajan and G. S. Yovanof, Noise estimation and filtering using block-based singular value decomposition, IEEE Transactions on Image Processing, 6, pp. 479-483, 1997.

12. K. Nakashima, Hybrid inspection system for LCD color filter panels, Proceedings of the 10th International Conference on Instrumentation and measurement Technology, Hamamatsu, pp. 689-692, 1994.
13. K. Kvaal, J. P. Wold, U. G. Indahl, P. Baardseth and T. Næs, Multivariate feature extraction from textural image of bread, Chemometrics and Intelligent Laboratory Systems, 42, pp. 141-158, 1998.
14. K. L. Chung, C. H. Shen and L. C. Chang, A novel SVD- and VQ-based image hiding scheme, Pattern Recognition Letters, 22, pp. 1051-1058, 2002.
15. L. P. Song and S. Y. Zhang, Singular value decomposition–based reconstruction algorithm for seismic traveltime tomography," IEEE Transactions on Image Processing, 8, pp. 1152-1154,1999.
16. M. A. Ibrahim, A. W. F. Hussein, S. A. Mashali and A. H. Mohamed, A blind image restoration system using higher-order statistics and random transform, IEEE International Conference on Electronics, Circuits and Systems, Lisboa, Portugal, 3, pp. 523-530, 1998.
17. M. Petrou and P. Bosdogianni, Image Processing, John Wiley & Sons, New York, NY, 1999.
18. P. O. Chen, S. H. Chen and F. C. Su, An effective method for evaluating the image-sticking effect of TFT-LCDs by interpretative modeling of optical measurements, Liquid Crystals, 27, pp. 965-975, 2000.
19. P. Waldemar, and T. A. Ramstad, Hybrid KLT-SVD image compression, Proceedings of IEEE International Conference on Acoustics, Speech, and Signal, Munich, Germany, 4, pp. 2713-2716, 1997.
20. R. J. Steriti and M. A. Fiddy, Regularized image reconstruction using SVD and a neural network method for matrix inversion, IEEE Transactions on Signal Processing, 41, pp. 3074-3077, 1993.
21. R. Liu and T. Tan, An SVD-based watermarking scheme for protecting rightful ownership, IEEE Transactions on Multimedia, 4, pp. 121-128, 2002.
22. S. Chandrasekaran, B. S. Manjunath, Y. F. Wang, J. Winkeler and H. Zhang, An eigenspace update algorithm for image analysis, Graphical Models and Image Processing, 59, pp. 321-332, 1997.
23. S. Hatipogly and S. K. Mitra, Texture feature extraction using Teager filters and singular value decomposition, International Conference on Consumer Electronics, Los Angeles, CA, pp. 440-441, 1998.

24. S. M. Sokolov and A. S. Treskunov, Automatic vision system for final test of liquid crystal display, Proceedings of the 1992 IEEE International Conference on Robotics and Automation, Nice, France, 1578-1582, 1992.
25. T. Kido, In-processing inspection technique for active-matrix LCD Panels, Proceedings of IEEE International Test Conference, Baltimore, MD, pp. 795-799, 1992.
26. T. Kido, N. Kishi and H. Takahashi, Optical charge-sensing method for testing and characterizing Thin-Film Transistor Arrays, IEEE Journal of Selected Topic in Quantum Electronics, 1, pp. 993-1001, 1995.
27. V. V. Selivanov and R. Lecomte, Fast PET image reconstruction based on SVD decomposition of the system matrix, IEEE Transactions on Nuclear Science, 48, pp. 761-767, 2001.
28. W. S. Hoge, E. L. Miller, H. Lev-Ari, D. H. Brooks, W. C. Karl and L. P. Panych, An efficient region of interest acquisition method for dynamic magnetic resonance imaging, IEEE Transactions on Image Processing, 10, pp. 1118-1128, 2001.

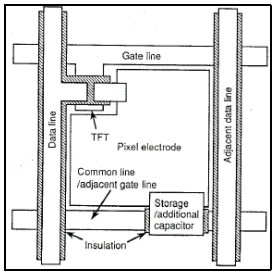

Figure 1. The schema of a single pixel of a TFT panel (source: see [26]).

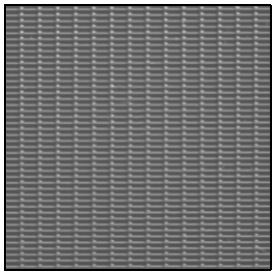

Figure 2. The surface image of a TFT panel.

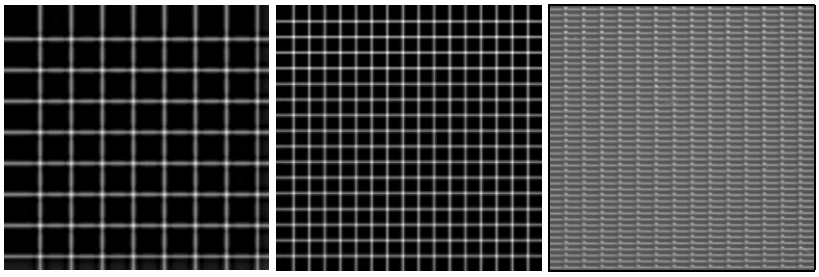

(a) (b) (c)

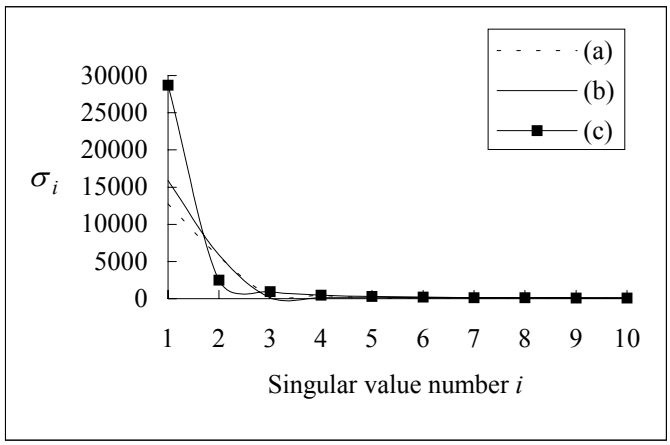

(d)

Figure 3. (a) and (b) Two artificial lines images with different line spacing; (c) a TFT panel image; (d) the plot of the corresponding first ten largest singular values.

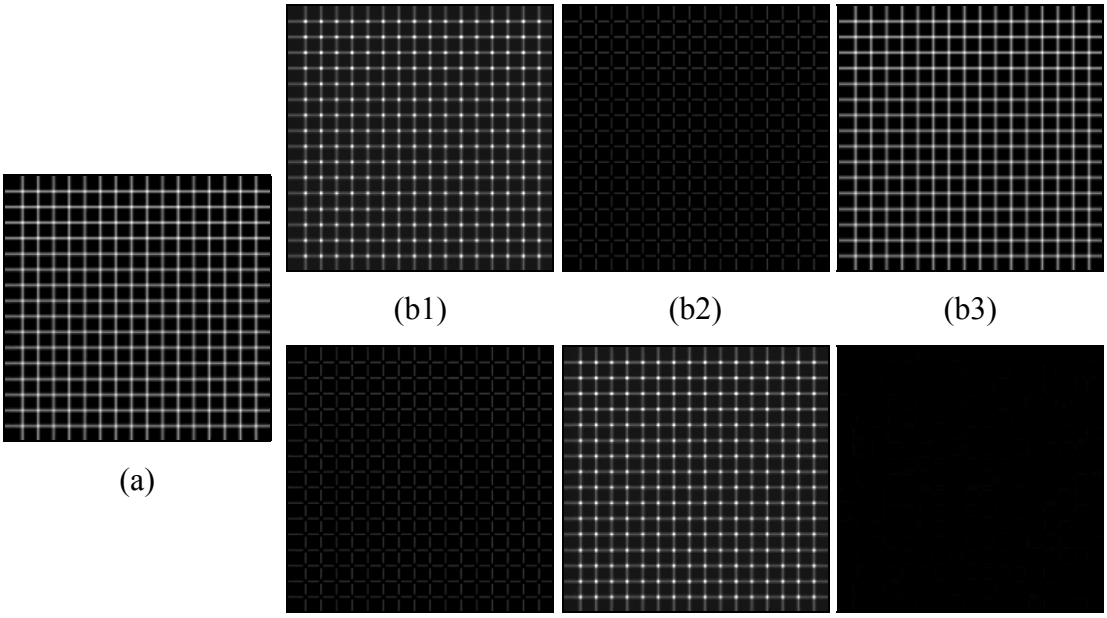

Figure 4. (a) The artificial horizontal/vertical lines image (the original image); (b1) the reconstructed image from σ_1; (b2) the reconstructed image from σ_2; (b3) the reconstructed image from both σ_1 and σ_2; (c1) the reconstructed image excluding σ_1; (c2) the reconstructed image excluding σ_2; (b3) the reconstructed image excluding both σ_1 and σ_2.

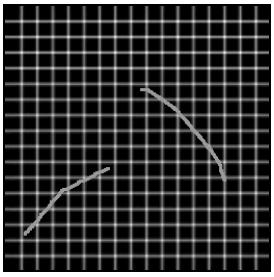

(a)

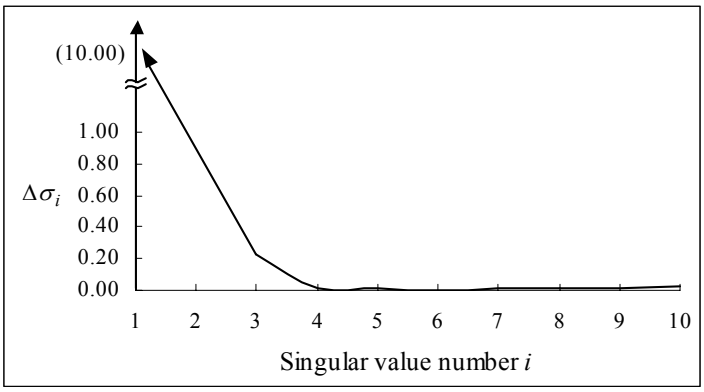

(b)

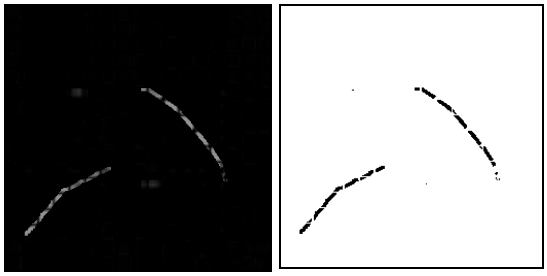

(c) (d)

Figure 5. The artificial orthogonal image with scratch defects:(a) the original image; (b) the plot of the marginal gain ($\Delta\sigma$) of normalized singular values; (c) the restored image; (d) the resulting binary image for defect segmentation.

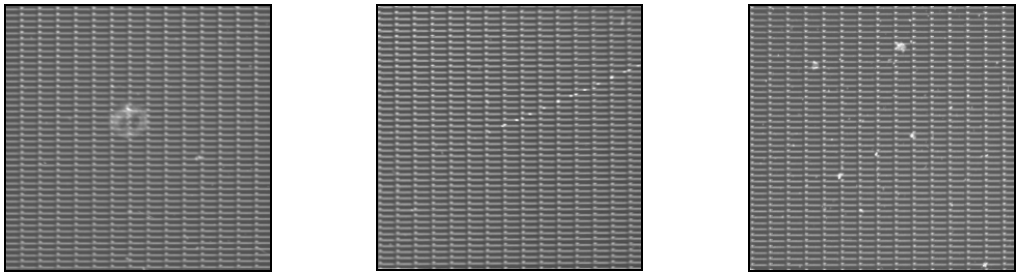

(a) (b) (c)

Figure 6. Three defective images under fine image resolution (60 pixels/mm): (a) pinhole; (b) scratch; (c) particle.

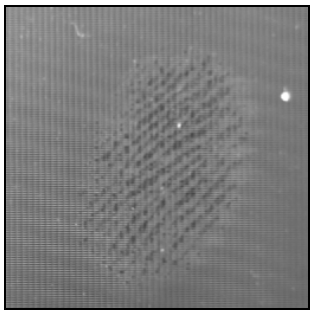

Figure 7. A defective image with fingerprint under coarse image resolution (20 pixels/mm).

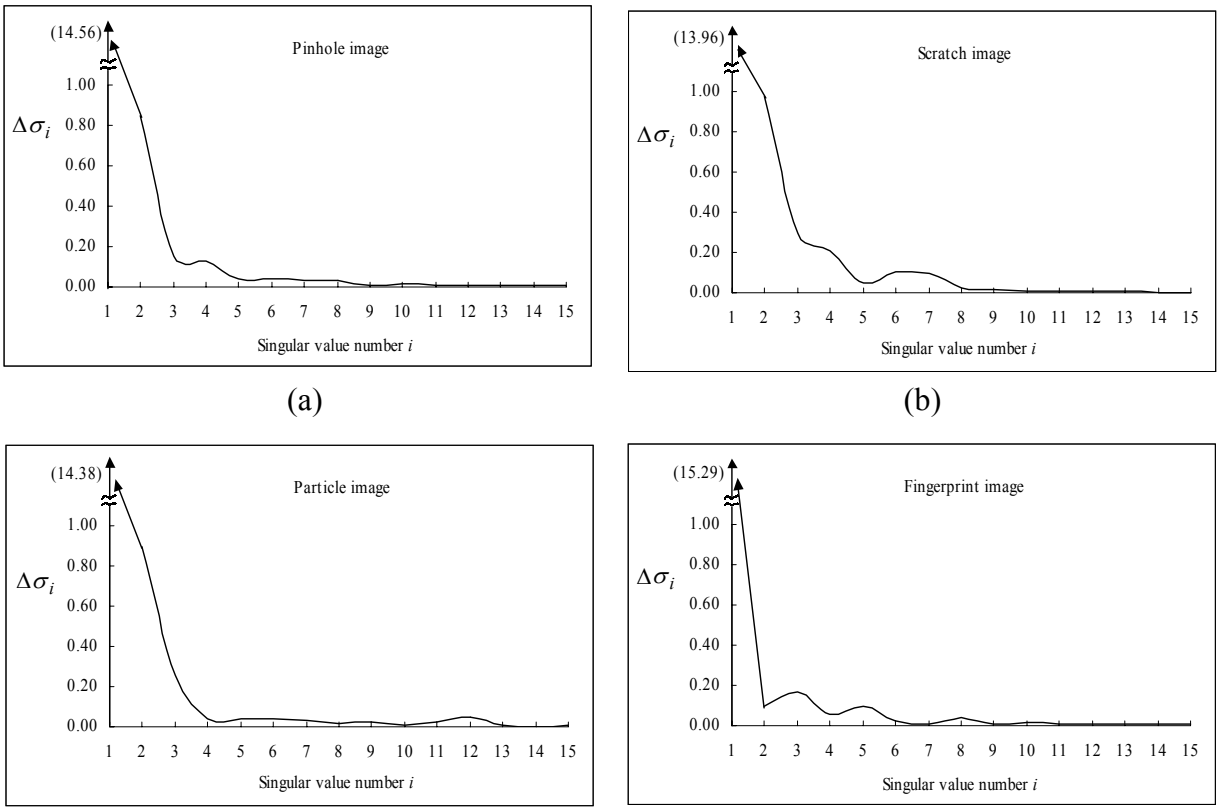

Figure 8. The plots of marginal gain ($\Delta\sigma$) of defective images: (a) the defective image of pinhole in Fig. 6(a); (b) the defective image of scratch in Fig. 6(b); (c) the defective image of particle in Fig. 6(c); (d) the defective image of fingerprint in Fig. 7.

Table 1. The normalized singular values and their marginal gains ($\Delta\sigma$) for the defective images in Figs. 6 and 7.

Defective image	Pinhole Fig. 6(a)		Scratch Fig. 6(b)		Particle Fig. 6(c)		Fingerprint Fig. 7	
Singular value (σ_i)	σ'	$\Delta\sigma$	σ'	$\Delta\sigma$	σ'	$\Delta\sigma$	σ'	$\Delta\sigma$
σ_1	15.86	14.56	15.77	13.96	15.83	14.38	15.89	15.29
σ_2	1.30	0.85	1.81	0.98	1.45	0.90	0.60	0.10
σ_3	0.45	0.15	0.83	0.30	0.55	0.26	0.51	0.17
σ_4	0.30	0.13	0.53	0.21	**0.30**	**0.04**	0.34	0.05
σ_5	**0.17**	**0.04**	0.32	0.05	0.25	0.04	0.29	0.10
σ_6	0.13	0.04	0.27	0.10	0.21	0.04	**0.19**	**0.02**
σ_7	0.09	0.03	0.17	0.10	0.17	0.03	0.17	0.01
σ_8	0.06	0.03	**0.07**	**0.02**	0.14	0.02	0.16	0.04
σ_9	0.03	0.01	0.05	0.02	0.12	0.03	0.12	0.01
σ_{10}	0.02	0.02	0.04	0.01	0.09	0.01	0.11	0.02

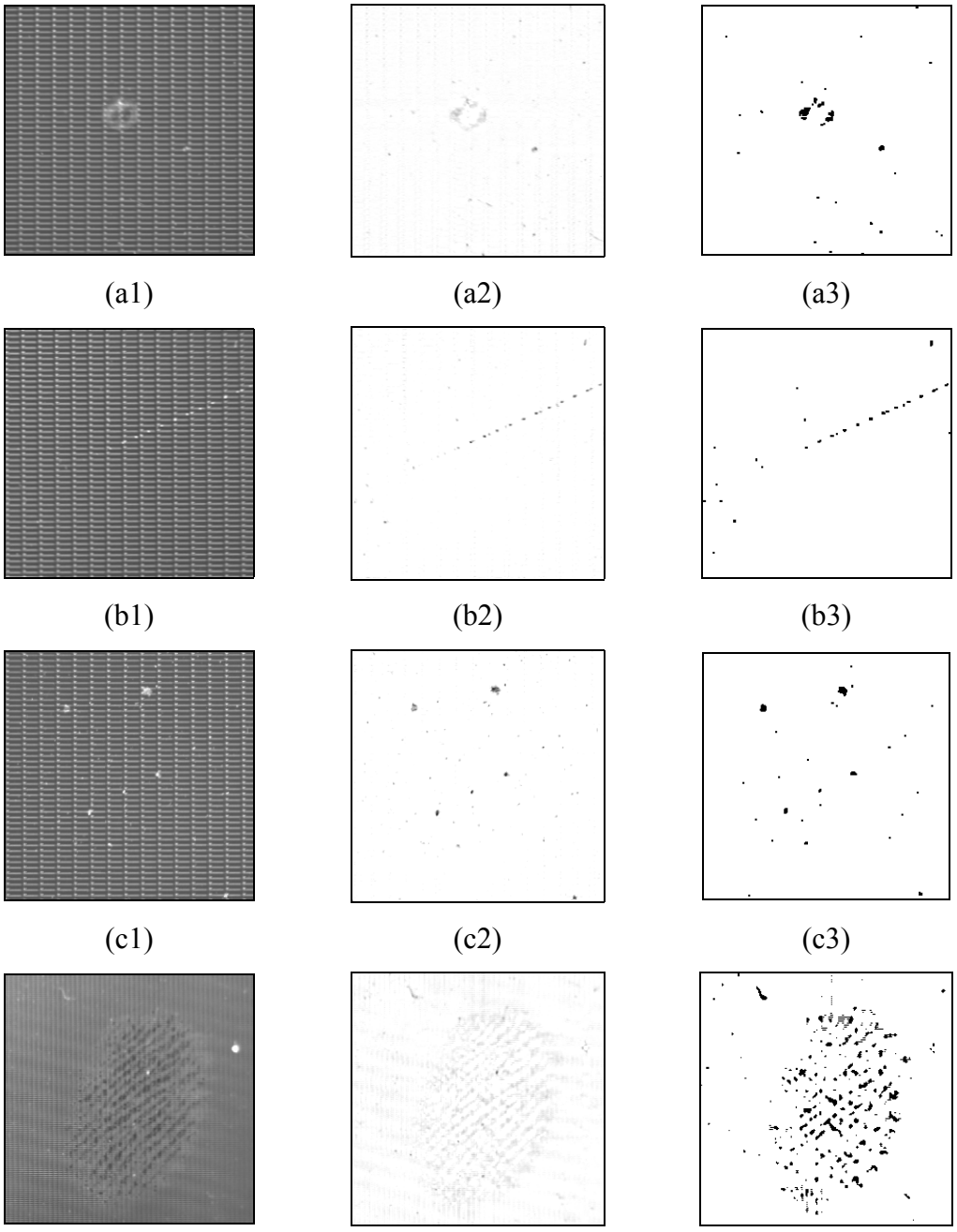

Figure 9. (a1)-(d1) The defective images with pinhole, scratch, particle and fingerprint, respectively; (a2)-(d2) the respective restored images; (a3)-(d3) the resulting binary images for defect segmentation.

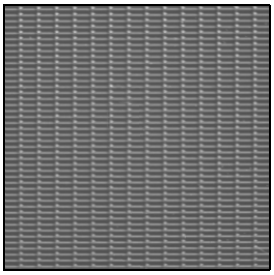

(a)

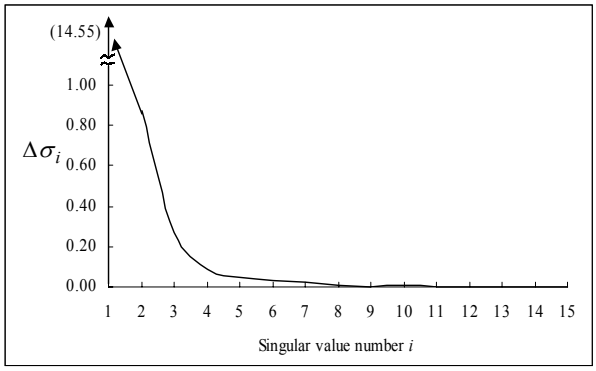

(b)

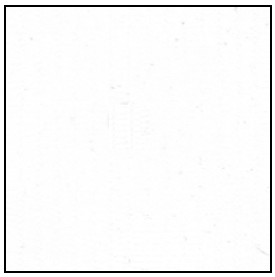

(c)

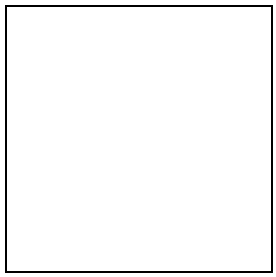

(d)

Figure 10. (a) A faultless version of the image in Fig. 6; (b) the plot of marginal gains ($\Delta\sigma$); (c) the restored image; (d) the resulting binary image.

Table 2. The normalized singular values and their marginal gains ($\Delta\sigma$) of the faultless image in Fig. 10(a).

Singular value (σ_i)	Faultless image in Fig. 10(a)	
	σ'	$\Delta\sigma$
σ_1	15.87	14.55
σ_2	1.31	0.87
σ_3	0.44	0.27
σ_4	0.17	0.09
σ_5	0.08	0.05
σ_6	**0.03**	**0.03**
σ_7	0.00	0.02
σ_8	-0.02	0.01
σ_9	-0.03	0.00
σ_{10}	-0.03	0.01

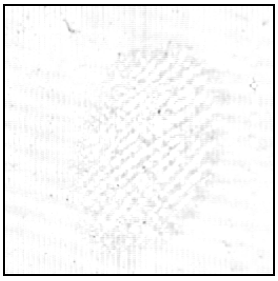

(a) $k = 6$

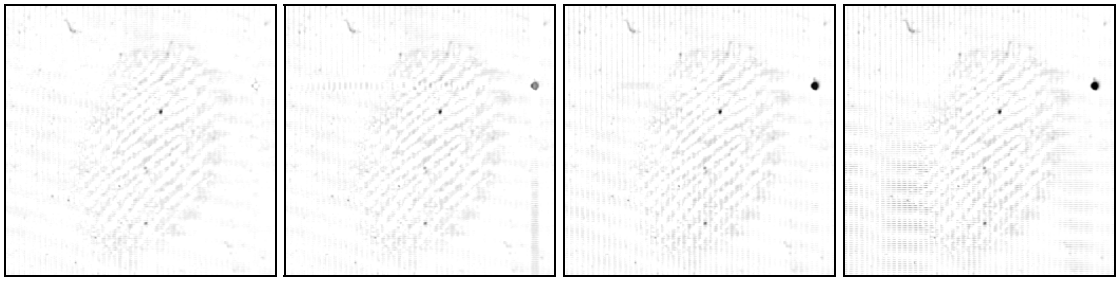

(b) $k-1$ (i.e., 5) (c) $k-2$ (i.e., 4) (d) $k-3$ (i.e., 3) (e) $k-4$ (i.e., 2)

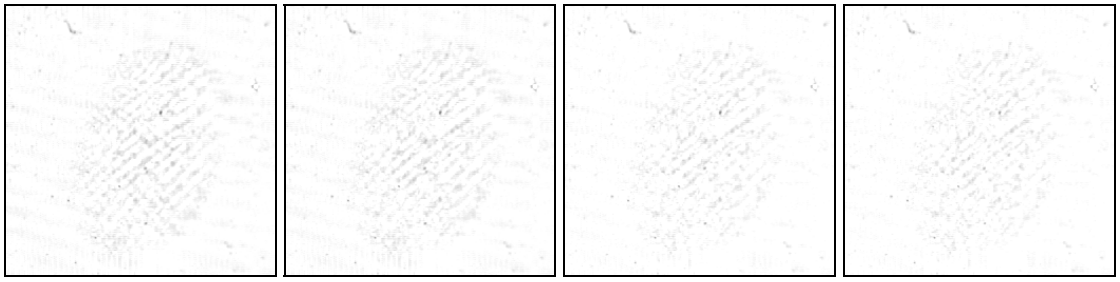

(f) $k+1$ (i.e., 7) (g) $k+2$ (i.e., 8) (h) $k+3$ (i.e., 9) (i) $k+4$ (i.e., 10)

Figure 11. The restored results of the fingerprint image in Fig. 7 from different selected numbers of singular values: (a) the result from $k = 6$; (b)-(e) the results from different selected numbers $k-1$, $k-2$, $k-3$ and $k-4$, respectively; (f)-(i) the results from different selected numbers $k+1$, $k+2$, $k+3$ and $k+4$, respectively.

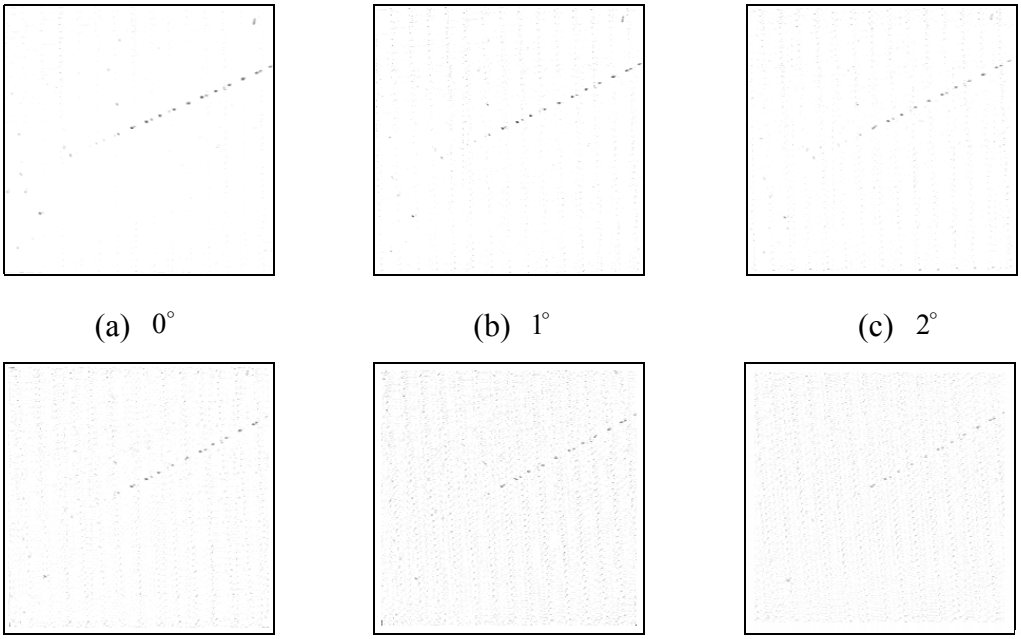

(a) 0° (b) 1° (c) 2°

(d) 3° (e) 4° (f) 5°

Figure 12. The restored results of the scratch image in Fig. 6 from various rotation angles: (a) the result from the original image; (b)–(f) the results from the images with 1°-, 2°-, 3°-, 4°- and 5°-rotation, respectively.